applied sciences

MDPI

Article

Circular Dichroism in Low-Cost Plasmonics: 2D Arrays of Nanoholes in Silver

Emilija Petronijevic [1,*], Alessandro Belardini [1], Grigore Leahu [1], Tiziana Cesca [2], Carlo Scian [2], Giovanni Mattei [2] and Concita Sibilia [1]

[1] Department S.B.A.I., Sapienza Università di Roma, Via A. Scarpa 14, I-00161 Rome, Italy; alessandro.belardini@uniroma1.it (A.B.); grigore.leahu@uniroma1.it (G.L.); concita.sibilia@uniroma1.it (C.S.)

[2] Physics and Astronomy Department, University of Padova, via Marzolo 8, I-35131 Padova, Italy; tiziana.cesca@unipd.it (T.C.); carlo.scian@unipd.it (C.S.); giovanni.mattei@unipd.it (G.M.)

* Correspondence: emilija.petronijevic@uniroma1.it

Received: 17 December 2019; Accepted: 12 February 2020; Published: 15 February 2020

Featured Application: chirality, plasmonics, enantioselectivity.

Abstract: Arrays of nanoholes in metal are important plasmonic devices, proposed for applications spanning from biosensing to communications. In this work, we show that in such arrays the symmetry can be broken by means of the elliptical shape of the nanoholes, combined with the in-plane tilt of the ellipse axes away from the array symmetry lines. The array then differently interacts with circular polarizations of opposite handedness at normal incidence, i.e., it becomes intrinsically chiral. The measure of this difference is called circular dichroism (CD). The nanosphere lithography combined with tilted silver evaporation was employed as a low-cost fabrication technique. In this paper, we demonstrate intrinsic chirality and CD by measuring the extinction in the near-infrared range. We further employ numerical analysis to visualize the circular polarization coupling with the nanostructure. We find a good agreement between simulations and the experiment, meaning that the optimization can be used to further increase CD.

Keywords: nanoholes; chirality; plasmonics; circular dichroism

1. Introduction

The physics of corrugated metal films has been attracting researchers for some decades now [1]. At the nanoscale, plasmonic arrays of nanoholes are able to couple light into plasmon oscillations at the metal-dielectric interface, i.e., surface plasmon polaritons (SPPs) [2]. These specific resonant electromagnetic excitations are strongly confined and lead to electromagnetic field enhancement at the interface [3]. Their resonant optical response is strongly influenced by the choice of the patterned metal, the materials surrounding it, and the periodicity of the array [4]. The unique coupling and subwavelength confinement properties of nanohole-based plasmonic devices have already led to many demonstrations and application proposals in subwavelength optics [5], surface enhanced Raman spectroscopy [6,7], enhanced fluorescence [8], emission rate modification [9], polarization conversion [10], and, in particular, chemical and biosensing [11–17].

One of the issues in plasmonic sensing is the ability to detect and characterize chirality, i.e., different interaction of the material with the left and right circularly polarized light (LCP and RCP, respectively). This difference can be characterized as normalized absorption difference between LCP and RCP, i.e., circular dichroism (CD). Chirality is a property of materials that lack mirror symmetry, and it is largely present in the molecules of many drugs. The two non-superimposable images of the same drug (so called enantiomers) are physically equal, but can have drastically different interactions

with the human body: while one acts as a drug, another can be toxic [18]. Therefore, one must be able to distinguish and eventually separate the "good" enantiomer from the "bad" one. Nowadays, the pharmaceutical industry could largely benefit from the improvements in chiral sensing that regard high sensitivity and low material waste. Plasmonics is promising for that matter as it can enhance interaction with electromagnetic fields at the nanoscale. Chirality can be designed [19] by breaking the symmetry in plasmonic nanomaterials during their fabrication, or with a proper oblique incidence set-up, as it was experimentally observed previously [20–24]. When a sample exhibits CD at normal incidence, it is said to be intrinsically chiral; on the contrary, in achiral samples the symmetry breaking can be induced by properly tilting the experimental set-up (extrinsic chirality). Furthermore, the enhanced enantioselectivity due to the enhanced near chiral fields was theoretically proposed in [25,26] and observed in the interaction with plasmonic substrates [27,28]. For this purpose, we previously proposed single hybrid GaAs-Au nanowires [29,30], periodic arrays of high refractive index nanowires [31], and arrays of Al nanopyramids [32]. Moreover, chiroptical responses were studied in simple 1D metal grooves [33] and nanohole arrays [34]. Most of the chiral nanostructure fabrication involves sophisticated, challenging and expensive techniques; however, authors in [35–37] showed that complex chiral shapes can be produced in silver films by a conventional single-pass focused ion beam technique.

In this work, we demonstrate that a low-cost nanosphere lithography (NSL) can be used to produce simple, yet intrinsically chiral, plasmonic nanohole arrays (NHA) in Ag. Starting from a self-assembled 2D metasurface of polystyrene nanospheres (PNSs), many high quality plasmonic nanostructures were fabricated [9,38–42]. Recently, we showed that the NSL approach combined with tilted metal deposition can lead to extrinsic chirality in hybrid polystyrene-metal metasurfaces [43], while authors in [44] used NSL to obtain giant CD in plasmonic nanocrescents. In [43] we noted that in the case of an Ag-polystyrene metasurface, a small in-plane tilt leads to a measurable CD, even at normal incidence. We further proposed PNS removal for the CD investigation in titled elliptical nanoholes. Therefore, in this work we study an Ag nanohole sample (Ag-NHA) where the PNSs were removed, leaving the elliptical nanohole array with triangular symmetry. We report on the CD in extinction in the 680–1000 nm range. We further fit the experimental data by numerical analysis and visualize the electromagnetic confinement in the nanohole vicinity. We believe that such a simple system can be further optimized to provide higher CD, and that the chiral molecules can be easily coupled with it for enantioselectivity measurements.

2. Materials and Methods

2.1. Fabrication

A 2D array of nanoholes in Ag with triangular symmetry was fabricated in a four-step process involving NSL and symmetry breaking. First, commercial PNSs (Microparticles GmbH, Berlin, Germany) with diameters of 518 nm were self-assembled into an ordered array on a glass substrate. The starting diameter defines the lattice periodicity of the final plasmonic structure. Next, reactive ion etching (RIE) with an Ar:O_2 mixture was used for the reduction of the initial PNS diameter to 356 nm, while preserving the ordered arrangement. This reduced diameter defines the short axis length of the final nanoellipse. Then, a layer of 55 nm of Ag was deposited by magnetron sputtering under an angle of 45°; an additional in-plane tilt of 28° was also introduced during this step. The Scanning Electron Microscopy (SEM) image of this sample is shown in Figure 1a. In [43] we characterized the chiral behavior of similar samples by means of photo-acoustic spectroscopy; moreover, we calculated the CD signal for the same geometry without PNSs with Ag semishells, and noticed CD improvement. This is due to the asymmetric shadow formed on the substrate during the oblique and tilted Ag deposition. Therefore, in the final step we removed PNSs by means of their dissolution in toluene; the SEM image after this step is shown in Figure 1b. The symmetry breaking in these arrays happens because of two effects: first, oblique metal deposition leads to the elliptical shape of the final nanohole, compared to the circular one with usual deposition (in the direction of the surface normal); second, the in-plane

tilt moves the ellipse axis away from the lines of hexagonal symmetry, as shown in the schematic in Figure 1c. The first effect is responsible for linear birefringence of the array of elliptic nanoholes, but it alone cannot lead to CD at normal incidence; if the elliptical axis is along the line of the lattice symmetry, such sample does not distinguish LCP from RCP. For CD we need an additional in-plane tilt, hence both first and second effects of the tilted Ag deposition. Moreover, we characterized the optical properties of the Ag layer by ellipsometric measurements, Figure 1d. As a reference for CD measurements, we also used a part of the sample that did not have PNSs, and this is why it contained only a flat layer of Ag (Ag-flat) on glass.

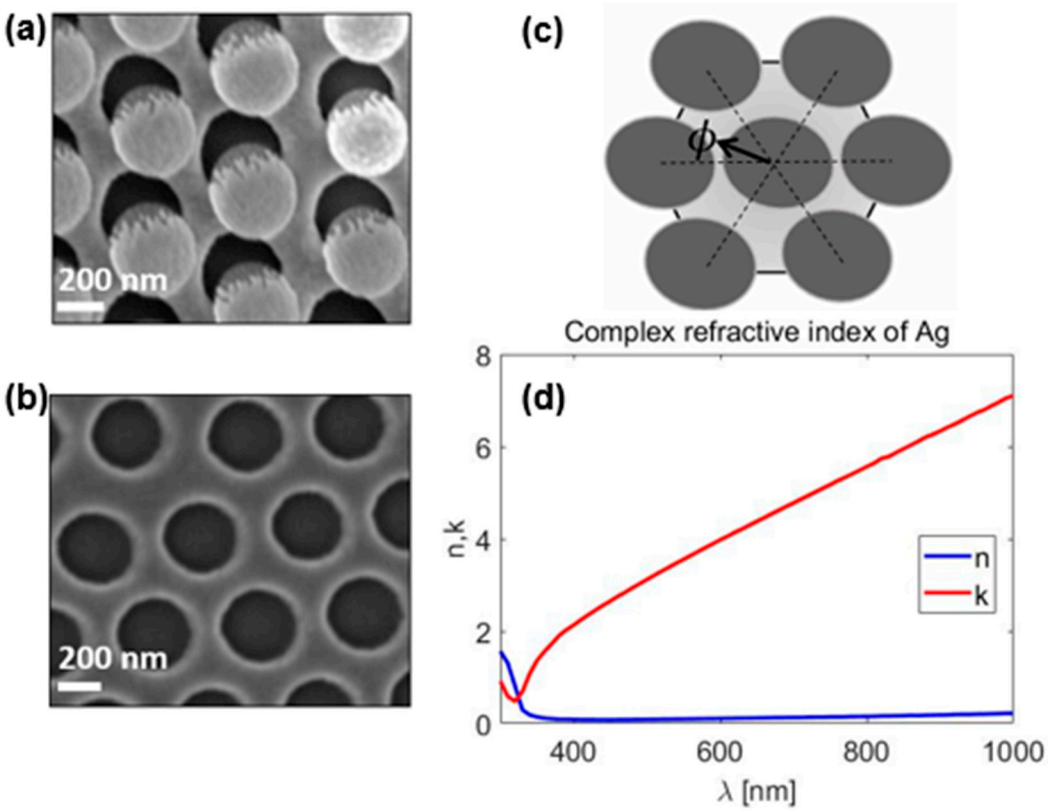

Figure 1. SEM image of the sample (**a**) before, and (**b**) after the PSN removal. (**c**) Schematic of the asymmetry due to the in-plane tilting of the elliptical nanoholes. (**d**) Ellipsometry characterization of the reference Ag film.

2.2. Measurements

The sample was characterized by using a widely tunable near-infrared laser (Chameleon Ultra II by Coherent Inc., Santa Clara, CA, USA). The pulse duration of this laser is 140 fs, with the repetition rate of 80 MHz. For linear characterization, we used a mechanical chopper at 70 Hz. Before impinging on the sample, the power was decreased by a beam-splitter (taking 4% of the output laser power) and a neutral density filter of 1.62. In Figure 2a the simplified experimental set-up is shown. The measurements are done at normal incidence, with laser light polarized in x-direction. The sample was aligned to have the short nanoellipse axis in x-direction, while the long axis (the Ag flux direction, projected in the xy-plane), was in y-direction. A quarter-wave plate was put on the light path before the sample in order to obtain circularly polarized light; the angles of its fast axis with respect to the y-direction were 0°, +45° and −45°, corresponding to linear polarization (x-polarized), RCP and LCP, respectively. The transmission was measured by a Si photodiode, and normalized to the one without the sample and quarter-wave plate. The results for the RCP and LCP circular polarizations incident upon Ag-NHA and Ag-flat are shown in Figure 2b; in the inset we show the response for linearly

polarized excitations (a y-polarized excitation is obtained by rotating the sample around *z*-axis for 90°). The laser power fluctuations were less than 0.5%, but a fixed part of the laser power (about 4%) was continuously (in real-time) monitored by using a beam splitter, in order to overcome fluctuation problems by using this part as a reference. In the short-wavelength and central zone of the spectrum (680–1000 nm), which is of interest for CD measurements in our sample, we also checked for a possible saturation effect of the detector, by measuring with different intensities of the laser, by using either neutral density 1.00 filter or neutral density 1.62 filter. The results were fully equivalent.

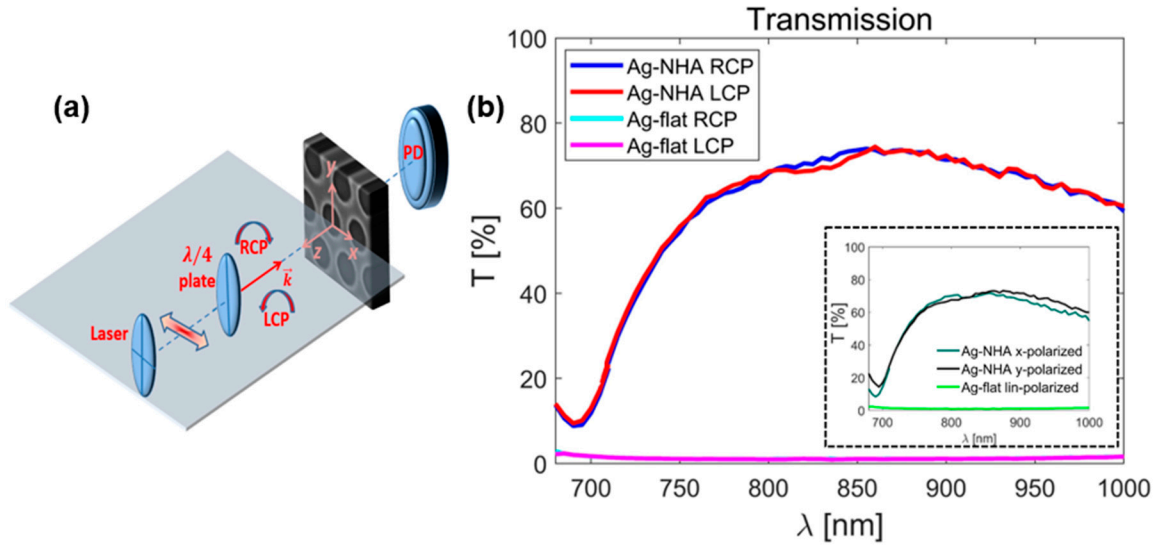

Figure 2. (**a**) Sketch of the experimental set-up; (**b**) Zero-order transmission spectra of the RCP and LCP light, exciting Ag-NHA and Ag-flat; inset: zero-order transmission spectra of linearly polarized light in x- and y-direction, exciting Ag-NHA and Ag-flat.

2.3. Simulations

The electromagnetic behavior of elliptic nanoholes was numerically investigated by the 3D Finite Difference Time Domain (FDTD) method by Lumerical [45]. To simulate the periodic array with triagonal symmetry, the unit cell was surrounded by periodic boundary conditions in the x- and y-directions, while perfectly matched layers were used in the z-direction. The lattice periodicity was fixed to $a = D_0 = 518$ nm, ellipse short diameter to D = 356 nm, and the ellipse was tilted for the in-plane angle from the triangular symmetry. NHA lay above a glass substrate, which was simulated as semi-infinite and lossless, with a refractive index of 1.517. As in the experiment, the excitation of the nanostructure was from the air-side, by two linearly polarized plane-wave sources; one was polarized in the direction of the long ellipse axis, and the other in the direction of the short one. To simulate RCP (LCP), a phase difference of π ($-\pi$) was defined between the sources. We further performed the same simulations for a flat Ag layer on glass.

3. Results

In the zero-order transmission (Figure 2b), there is a clear resonant dip around 693 nm, followed by a region of higher transmission for both circular and both linear polarizations. In the case of linearly polarized light, one can apply the formula for the SPPs between Ag and glass for the trigonal symmetry [14]. Considering the experimental values of Ag permittivity, we find that the transmission dip closely coincides with the lowest order Ag-glass SPP (~695 nm), while it is slightly red-shifted from Wood's anomaly. Strong interaction of this SPP with the lattice diffraction mode resulted in transmission minimum [46]. As can be noted from the inset of the Figure 2b, two perpendicular linear polarizations differently interact with Ag-NHA, which is expected due to the elliptical shape of the

nanoholes. However, this linear dichroism is a necessary, but not sufficient, condition for CD, which can eventually be enabled by the nanohole tilt. Both RCP and LCP spectra "carry" the resonance of the x- and y-polarized excitations, as they are partially excited by the light coupled to the aforementioned mode. Moreover, we note some differences between LCP and RCP transmission in the 800–860 nm range. However, chirality and CD are usually characterized as the difference in absorption, or, in our case, extinction ($Ext_{RCP,LCP} = 1 - T_{RCP,LCP}$). In Figure 3a we report on the experimental extinction for LCP and RCP excitations, for Ag-NHA and Ag-flat. We further define CD as the normalized difference in the extinction between LCP and RCP:

$$CD_{Ext}[\%] = 100 \cdot \frac{Ext_{LCP} - Ext_{RCP}}{Ext_{LCP} + Ext_{RCP}}.$$

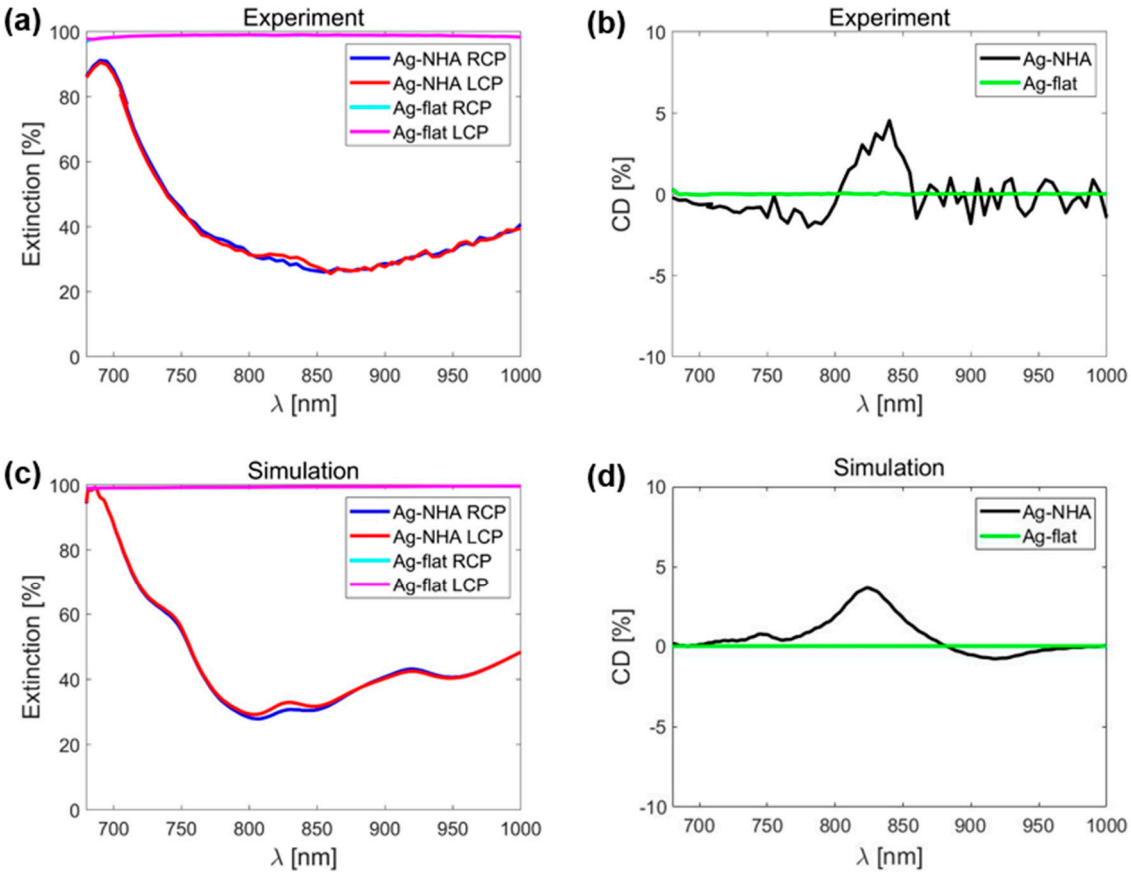

Figure 3. Experimental results for Ag-NHA and Ag-flat: (**a**) extinction spectra for RCP and LCP excitation, and (**b**) CD. Simulations for Ag-NHA and Ag-flat: (**c**) extinction spectra for RCP and LCP excitation, and (**d**) CD.

Spectral characterization in Figure 3b shows that CD for Ag-NHA has a maximum of ~5% around 825 nm, and while approaching the resonance it decreases close to 0. This is due to the normalized extinction differences: close to the SPP resonance, both RCP and LCP at normal incidence have a high extinction peak, so that their normalized difference tends to be zero. In the range of low extinction, the differences are noticeable, thus enhancing the CD. As expected, Ag-flat does not distinguish between RCP and LCP, giving CD = 0 in the whole spectral range. Simulated extinction for Ag-flat and Ag-NHA in Figure 3c gives good agreement with the experiments reported above in terms of the shape and intensities. However, the discrepancy is notable as the simulation assumes a perfectly uniform periodic structure with well-defined nanoellipse, while from SEM measurements (see Figure 1b) we note size and shape variations of the nanoholes. We believe that the reason why in the experiment the spectra

are flatter (without multiple features) could be as a result of the averaging of the responses of slightly different nanoholes. Figure 3d shows that the ideal simulated case leads to CD that closely resembles the measured one in Figure 3b.

It is important to numerically investigate the origin of the CD behavior. The electromagnetic field behavior can be visualized as a 3D absorption density ρ_{abs} in the unit cell [43]. In Figure 4, the extinction maximum wavelength is investigated, i.e., 693 nm. As expected, the electromagnetic field is enhanced and confined at the interface between the nanoholes and the glass substrate, but the absorption density does not show an evident difference between RCP and LCP. The same color scale is kept and ρ_{abs} is visualized at CD maximum wavelength of 825 nm. First, it is evident that the overall absorption is lower for both excitations compared to the previous, resonant one; moreover, the field is not confined to the glass-Ag interface. However, here the LCP excitation gets more absorbed, as it is evident from the rims of the nanoholes in the bottom right corner of Figure 4. It therefore gives a positive CD, as seen from Figure 3. For future work, CD in absorption will be monitored by photo-acoustic spectroscopy, which we previously applied for the characterization of SPPs in achiral nanohole arrays in gold [47].

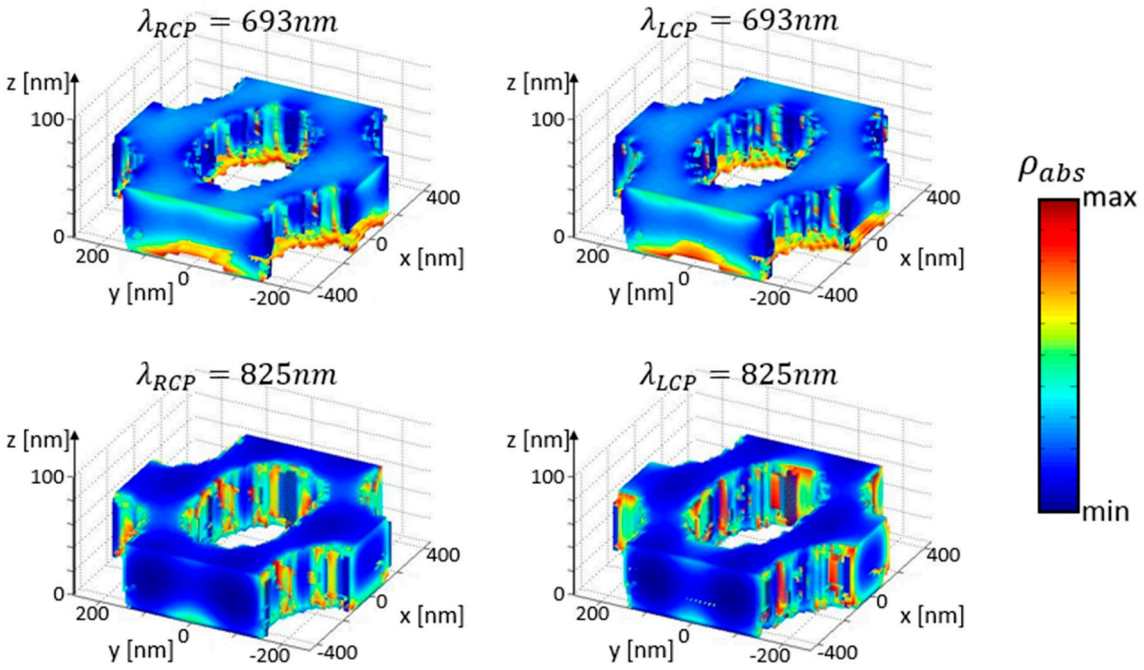

Figure 4. Simulated absorption densities for RCP and LCP excitations at the resonant wavelength (693 nm) and the maximum CD wavelength (825 nm). The color scale is equal for all distributions.

4. Discussion

We highlight that the spectral characterization of CD is needed in order to visualize resonant and non-resonant contributions in the nanomaterials with broken symmetry. Even though our sample was produced by a low-cost, self-assembling technique, the overall uniformity provided non-zero CD signal at normal incidence. Once the nanostructure is simulated and a good agreement with the experiment is found, one can optimize the unit cell geometry and materials to provide CD in the specific wavelength range, and of higher absolute value. We believe that bringing together the advantages of a low-cost fabrication technique and chirality in simple nanohole samples could lead to easier coupling of plasmonic substrates and chiral molecules, and hence enrich the world of chiral sensing.

Author Contributions: Conceptualization, E.P. and A.B.; Methodology, C.S. (Concita Sibilia); Software, A.B. and G.L.; Validation, T.C., G.M. and C.S. (Carlo Scian); Formal analysis, E.P.; Investigation, E.P. and A.B.; Resources, C.S. (Carlo Scian), T.C. and G.M.; Data curation, E.P.; Writing—original draft preparation, E.P.; Writing—review and editing, A.B., T.C. and C.S. (Concita Sibilia); Visualization, E.P.; Supervision, G.L. and C.S. (Concita Sibilia);

Project administration, C.S. (Concita Sibilia); Funding acquisition, C.S. (Concita Sibilia). All authors have read and agreed to the published version of the manuscript.

Funding: This research received no external funding.

Acknowledgments: Part of the measurements were performed by using the LASAFEM facility (cofounded by Sapienza Università di Roma, Infrastructure Project prot. n. MA31715C8215A268 and by Italian Ministry of Defence, SCHERMA project contr. n. 1880 rep. 22/12/2016).

Conflicts of Interest: The authors declare no conflict of interest.

References

1. Ebbesen, T.W.; Lezec, H.J.; Ghaemi, H.F.; Thio, T.; Wolff, P.A. Extraordinary optical transmission through sub-wavelength hole arrays. *Nature* **1998**, *391*, 667. [CrossRef]
2. Maier, S.A. *Plasmonics: Fundamentals and A*; pplications Springer Science & Business: Media, Germany, 2007.
3. Salomon, L.; Grillot, F.; Zayats, A.V.; de Fornel, F. Near-Field Distribution of Optical Transmission of Periodic Subwavelength Holes in a Metal Film. *Phys. Rev. Lett.* **2001**, *86*, 1110. [CrossRef] [PubMed]
4. García de Abajo, F.J. Colloquium: Light scattering by particle and hole arrays. *Rev. Mod. Phys.* **2007**, *79*, 1267. [CrossRef]
5. Barnes, W.L.; Dereux, A.; Ebbesen, T.W. Surface plasmon subwavelength optics. *Nature* **2003**, *424*, 824. [CrossRef]
6. Xu, J.; Guan, P.; Kvasnička, P.; Gong, H.; Homola, J.; Yu, Q. Light Transmission and Surface-Enhanced Raman Scattering of Quasi-3D Plasmonic Nanostructure Arrays with Deep and Shallow Fabry-Pérot Nanocavities. *J. Phys. Chem. C* **2011**, *115*, 10996–11002. [CrossRef]
7. Masson, J.-F.; Murray-Methota, M.-P.; Livea, L.S. Nanohole arrays in chemical analysis: manufacturing methods and applications. *Analyst* **2010**, *135*, 1483–1489. [CrossRef]
8. Brolo, A.G.; Kwok, S.C.; Moffitt, M.G.; Gordon, R.; Riordon, J.; Kavanagh, K.L. Enhanced Fluorescence from Arrays of Nanoholes in a Gold Film. *J. Am. Chem. Soc.* **2005**, *127*, 14936–14941. [CrossRef]
9. Michieli, N.; Kalinic, B.; Scian, C.; Cesca, T.; Mattei, G. Emission Rate Modification and Quantum Efficiency Enhancement of Er3+ Emitters by Near-Field Coupling with Nanohole Arrays. *ACS Photonics* **2018**, *5*, 2189–2199. [CrossRef]
10. Cao, Z.L.; Yiu, L.Y.; Zhang, Z.Q.; Chan, C.T.; Ong, H.C. Understanding the role of surface plasmon polaritons in two-dimensional achiral nanohole arrays for polarization conversion. *Phys. Rev. B* **2017**, *95*, 155415. [CrossRef]
11. Blanchard-Dionne, A.; Meunier, M. Sensing with periodic nanohole arrays. *Adv. Opt. Photon.* **2017**, *9*, 891–940. [CrossRef]
12. Escobedo, C. On-chip nanohole array based sensing: a review. *Lab. Chip.* **2013**, *13*, 2445. [CrossRef] [PubMed]
13. Balaşa, I.G. Nano-Hole Arrays for plasmonic biosensors. Master's Degree Thesis, University of Padova, via Marzolo 8, I-35131 Padova, Italy, 2015.
14. Couture, M.; Liang, Y.; Poirier Richard, H.-P.; Faid, R.; Peng, W.; Masson, J.-F. Tuning the 3D plasmon field of nanohole arrays. *Nanoscale* **2013**, *5*, 12399. [CrossRef] [PubMed]
15. Jia, P.; Jiang, H.; Sabarinathan, J.; Yang, J. Plasmonic nanohole array sensors fabricated by template transfer with improved optical performance. *Nanotechnology* **2013**, *24*, 195501. [CrossRef] [PubMed]
16. Blanchard-Dionne, A.; Meunier, M. Multiperiodic nanohole array for high precision sensing. *Nanophotonics* **2018**, *8*, 325–329. [CrossRef]
17. Valsecchi, C.; Gomez Armas, L.E.; Weber de Menezes, J. Large Area Nanohole Arrays for Sensing Fabricated by Interference Lithography. *Sensors* **2019**, *19*, 2182. [CrossRef]
18. Nguyen, L.A.; He, H.; Pham-Huy, C. Chiral drugs: An overview. *Adv. Nat. Sci. Nanosci. Nanotechnol.* **2006**, *2*, 85–100.
19. Schäferling, M.; Dregely, D.; Hentschel, M.; Giessen, H. Tailoring enhanced optical chirality: Design principles for chiral plasmonic nanostructures. *Phys. Rev. X* **2012**, *2*, 031010. [CrossRef]
20. Belardini, A.; Larciprete, M.C.; Centini, M.; Fazio, E.; Sibilia, C.; Chiappe, D.; Martella, C.; Toma, A.; Giordano, M.; Buatier de Mongeot, F. Circular dichroism in the optical second-harmonic emission of curved gold metal nanowires. *Phys. Rev. Lett.* **2011**, *107*, 257401. [CrossRef]

21. Belardini, A.; Centini, M.; Leahu, G.; Hooper, D.C.; Li Voti, R.; Fazio, E.; Haus, J.W.; Sarangan, A.; Valev, V.K.; Sibilia, C. Chiral light intrinsically couples to extrinsic/pseudo-chiral metasurfaces made of tilted gold nanowires. *Sci. Rep.* **2016**, *6*, 31796. [CrossRef]
22. Leahu, G.; Petronijević, E.; Belardini, A.; Centini, M.; Sibilia, C.; Hakkarainen, T.; Koivusalo, E.; Rizzo Piton, M.; Suomalainen, S.; Guina, M. Evidence of Optical Circular Dichroism in GaAs-Based Nanowires Partially Covered with Gold. *Adv. Opt. Mater.* **2017**, *5*, 1601063. [CrossRef]
23. Petronijević, E.; Leahu, G.; Belardini, A.; Centini, M.; Li Voti, R.; Hakkarainen, T.; Koivusalo, E.; Rizzo Piton, M.; Suomalainen, S.; Guina, M.; et al. Photo-Acoustic Spectroscopy Reveals Extrinsic Optical Chirality in GaAs-Based Nanowires Partially Covered with Gold. *Int. J. Thermophys.* **2018**, *39*, 45. [CrossRef]
24. Hakkarainen, T.; Petronijević, E.; Rizzo Piton, M.; Sibilia, C. Demonstration of extrinsic chirality of photoluminescence with semiconductor-metal hybrid nanowires. *Sci. Rep.* **2019**, *9*, 5040. [CrossRef] [PubMed]
25. Tang, Y.; Cohen, A.E. Optical chirality and its interaction with matter. *Phys. Rev. Lett.* **2010**, *104*, 163901. [CrossRef]
26. Tang, Y.; Cohen, A.E. Enhanced enantioselectivity in excitation of chiral molecules by superchiral light. *Science* **2011**, *332*, 333–336. [CrossRef]
27. Hendry, E.; Carpy, T.; Johnston, J.; Popland, M.; Mikhaylovskiy, R.V.; Lapthorn, A.J.; Kelly, S.M.; Barron, L.D.; Gadegaard, N.; Kadodwala, M. Ultrasensitive detection and characterization of biomolecules using superchiral fields. *Nat. Nanotechnol.* **2010**, *5*, 783–787. [CrossRef] [PubMed]
28. Zhao, Y.; Askarpour, A.N.; Sun, L.; Shi, J.; Li, X.; Alù, A. Chirality detection of enantiomers using twisted optical metamaterials. *Nat. Commun.* **2017**, *8*, 14180. [CrossRef]
29. Petronijević, E.; Centini, M.; Belardini, A.; Leahu, G.; Hakkarainen, T.; Sibilia, C. Chiral near-field manipulation in Au-GaAs hybrid hexagonal nanowires. *Opt. Express* **2017**, *25*, 14148. [CrossRef] [PubMed]
30. Leahu, G.; Petronijević, E.; Belardini, A.; Centini, M.; Li Voti, R.; Hakkarainen, T.; Koivusalo, E.; Guina, M.; Sibilia, C. Photo-acoustic spectroscopy revealing resonant absorption of self-assembled GaAs-based nanowires. *Sci. Rep.* **2017**, *7*, 2833. [CrossRef] [PubMed]
31. Petronijević, E.; Sibilia, C. Enhanced Near-Field Chirality in Periodic Arrays of Si Nanowires for Chiral Sensing. *Molecules* **2019**, *24*, 853. [CrossRef]
32. Petronijević, E.; Sandoval, E.M.; Ramezani, M.; Ordóñez-Romero, C.L.; Noguez, C.; Bovino, F.A.; Sibilia, C.; Pirruccio, G. Extended Chiro-optical Near-Field Response of Achiral Plasmonic Lattices. *J. Phys. Chem. C* **2019**, *123*, 38–23620. [CrossRef]
33. Yao, H.; Zhong, S. Handedness-switchable chiral field in the 1D metal grooves for plasmonic circular dichroism spectroscopy. *J. Opt.* **2017**, *19*, 055001. [CrossRef]
34. Maoz, B.M.; Ben Moshe, A.; Vestler, D.; Bar-Elli, O.; Markovich, G. Chiroptical Effects in Planar Achiral Plasmonic Oriented Nanohole Arrays. *Nano Lett.* **2012**, *12*, 2357–2361. [CrossRef] [PubMed]
35. Gorkunov, M.V.; Ezhov, A.A.; Artemov, V.V.; Rogov, O.Y.; Yudin, S.G. Extreme optical activity and circular dichroism of chiral metal hole arrays. *Appl. Phys. Lett.* **2014**, *104*, 221102. [CrossRef]
36. Gorkunov, M.V.; Dmitrienko, V.E.; Ezhov, A.A.; Artemov, V.V.; Rogov, O.Y. Implications of the causality principle for ultra chiral metamaterials. *Sci. Rep.* **2015**, *5*, 9273. [CrossRef] [PubMed]
37. Kondratov, A.V.; Gorkunov, M.V.; Darinskii, A.N.; Gainutdinov, R.V.; Rogov, O.Y.; Ezhov, A.A.; Artemov, V.V. Extreme optical chirality of plasmonic nanohole arrays due to chiral Fano resonance. *Phys. Rev. B* **2016**, *93*, 195418. [CrossRef]
38. Cesca, T.; Michieli, N.; Kalinic, B.; Sánchez-Espinoza, A.; Rattin, M.; Russo, V.; Mattarello, V.; Scian, C.; Mazzoldi, P.; Mattei, G. Nonlinear absorption tuning by composition control in bimetallic plasmonic nanoprism arrays. *Nanoscale* **2015**, *7*, 12411–12418. [CrossRef]
39. Russo, V.; Michieli, N.; Cesca, T.; Scian, C.; Silvestri, D.; Morpurgo, M.; Mattei, G. Gold–silver alloy semi-nanoshell arrays for label-free plasmonic biosensors. *Nanoscale* **2017**, *9*, 10117–10125. [CrossRef]
40. Sanchez-Esquivel, H.; Raygoza-Sanchez, K.Y.; Rangel-Rojo, R.; Gemo, E.; Michieli, N.; Kalinic, B.; Reyes-Esqueda, J.A.; Cesca, T.; Mattei, G. Spectral dependence of nonlinear absorption in ordered silver metallic nanoprism arrays. *Sci. Rep.* **2017**, *7*, 5307.
41. Sanchez-Esquivel, H.; Raygoza-Sanchez, K.Y.; Rangel-Rojo, R.; Kalinic, B.; Michieli, N.; Cesca, T.; Mattei, G. Ultra-fast dynamics in the nonlinear optical response of silver nanoprisms ordered arrays. *Nanoscale* **2018**, *10*, 5182–5190. [CrossRef]

42. Cesca, T.; Garcia Ramirez, E.V.; Sanchez-Esquivel, H.; Michieli, N.; Kalinic, B.; Gomez Cervantes, J.M.; Rangel-Rojo, R.; Reyes Esqueda, J.A.; Mattei, G. Dichroic nonlinear absorption response of silver nanoprism arrays. *RSC Adv.* **2017**, *7*, 17741–17747. [CrossRef]
43. Petronijević, E.; Leahu, G.; Li Voti, R.; Belardini, A.; Scian, C.; Michieli, N.; Cesca, T.; Mattei, G.; Sibilia, C. Photo-acoustic detection of chirality in metal-polystyrene metasurfaces. *Appl. Phys. Lett.* **2019**, *114*, 053101. [CrossRef]
44. Wang, Y.; Qi, J.; Pan, C.; Wu, Q.; Yao, J.; Chen, Z.; Chen, J.; Li, Y.; Yu, X.; Sun, Q.; et al. Giant circular dichroism of large-area extrinsic chiral metal nanocrecents. *Sci. Rep.* **2018**, *8*, 3351. [CrossRef] [PubMed]
45. Lumerical Solutions, Inc. Available online: http://www.lumerical.com/tcad-products/fdtd/ (accessed on 11 January 2019).
46. Huang, C.; Wang, Q.; Zhu, Y. Dual effect of surface plasmons in light transmission through perforated metal films. *Phys. Rev. B* **2007**, *75*, 245421. [CrossRef]
47. Petronijević, E.; Leahu, G.; Mussi, V.; Sibilia, C.; Bovino, A.F. Photoacoustic technique for the characterization of plasmonic properties of 2D periodic arrays of gold nanoholes. *AIP Adv.* **2017**, *7*, 025210. [CrossRef]